Liquid Crystals
Publication details, including instructions for authors and subscription information:
http://www.informaworld.com/smpp/title~content=t713926090

Simulation of dynamic response to an electric field of surface stabilized antiferroelectric liquid crystals

Tadashi Akahane[a]; Atsushi Obinata[a]
[a] Department of Electrical Engineering, Faculty of Engineering, Nagaoka University of Technology, Niigata, Japan

To cite this Article Akahane, Tadashi and Obinata, Atsushi(1993) 'Simulation of dynamic response to an electric field of surface stabilized antiferroelectric liquid crystals', Liquid Crystals, 15: 6, 883 — 892
To link to this Article: DOI: 10.1080/02678299308036507
URL: http://dx.doi.org/10.1080/02678299308036507

LIQUID CRYSTALS, 1993, VOL. 15, NO. 6, 883–892

Simulation of dynamic response to an electric field of surface stabilized antiferroelectric liquid crystals†

by TADASHI AKAHANE* and ATSUSHI OBINATA
Department of Electrical Engineering, Faculty of Engineering,
Nagaoka University of Technology, Kamitomioka 1603-1,
Nagaoka, Niigata 940-21, Japan

(*Received 25 June 1992; accepted 21 May 1993*)

Responses of surface stabilized antiferroelectric liquid crystals (SSAFLCs) to an electric field are simulated based on a model of the AFLC phase. The apparent tilt angle, the polarization reversal current and the optical transmission under applied triangular wave voltages are calculated. The results obtained systematically explain the experimental observations fairly well. The effects of parameters such as amplitude and frequency of applied voltages, an antiferroelectric coupling parameter and surface anchoring strength on these phenomena are discussed.

1. Introduction

Since the observation of antiferroelectricity in MHPOBC [1], much attention has been paid to antiferroelectric liquid crystals (AFLCs) from both practical and fundamental points of view. They show double hysteresis in D–E curves [2] and in the electric field dependence of the apparent optical tilt angle [3]. When a triangular wave voltage is applied, double peaks are generally observed in the polarization reversal current [4]. These phenomena are all due to the tri-stable switching amongst an antiferroelectic state and two uniform ferroelectric states.

The structure of ALFC is considered to consist of two ferroelectric S_C^* sublattices which are paired by antiferroelectric coupling. Based on this model, we calculate the apparent optical tilt angle, the polarization reversal current and the optical transmission under applied triangular voltages. The effects of parameters such as amplitude and frequency of applied voltages, an antiferroelectric coupling parameter and surface anchoring strength on these phenomena are discussed.

2. Model and free energy density of AFLCs

In the antiferroelectric smectic C_A^* phase of an AFLC material, the polarization vectors in adjacent layers are antiparallel and rotate about the layer normal to form a helical structure, in the same manner as that in a ferroelectric S_C^* phase. Therefore, the structure of the AFLC phase is considered to consist of two ferroelectric sublattices (odd-numbered layers and even-numbered layers) which are paired by antiferroelectic coupling [5]. We assume that the antiferroelectric coupling energy density is given by

$$f_0 = \alpha \mathbf{P}_1 \cdot \mathbf{P}_2, \tag{1}$$

where $\mathbf{P}_1$ and $\mathbf{P}_2$ are the spontaneous polarizations in odd-numbered layers and even-numbered layers, respectively. The amplitude of $\mathbf{P}_1$ and $\mathbf{P}_2$ are equal and we put $P_1 = P_2 = P_s/2$. The S_{CA}^* or S_C^* phase is stabilized according to $\alpha > 0$ or $\alpha < 0$.

* Author for correspondence.

† Presented at the Fourteenth International Liquid Crystal Conference, 21–26 June 1992, University of Pisa, Italy.

0267–8292/93 $10·00

The elastic free energy density of S_{CA}^* is considered to be the sum of those of S_C^* sublattices. Using the **c** director expression of the elastic free energy density of S_C^* proposed by Dahl and Lagerwall [6], we have

$$f_{\text{elas}} = \sum_{i=1}^{2} \Big(\tfrac{1}{4}B_1\{\mathbf{k}\cdot(\nabla\times\mathbf{c}_i)\}^2 + \tfrac{1}{4}B_2(\nabla\cdot\mathbf{c}_i)^2 + \tfrac{1}{4}B_3\{\mathbf{c}_i\cdot(\nabla\times\mathbf{c}_i)\}^2 - \tfrac{1}{2}B_{13}\{\mathbf{k}\cdot(\nabla\times\mathbf{c}_i)\}\{\mathbf{c}_i\cdot(\nabla\times\mathbf{c}_i)\} + \tfrac{1}{2}D_1\{\mathbf{k}\cdot(\nabla\times\mathbf{c}_i)\} - \tfrac{1}{2}D\{\mathbf{c}_i\cdot(\nabla\times\mathbf{c}_i)\} \Big), \tag{2}$$

where **k** is the unit vector along the layer normal, and $\mathbf{c}_1$, $\mathbf{c}_2$ are **c** directors in odd-numbered layers and in even-numbered layers, respectively. Equation (2) describes the elastic energy of the distortion of the **c** director. The layer distortion is not considered here. Equation (2) reduces to that of S_C^* when $\mathbf{c}_1 = \mathbf{c}_2 = \mathbf{c}$.

The dielectric free energy density is given by

$$f_{\text{d}} = -\tfrac{1}{2}\mathbf{D}\cdot\mathbf{E} = -\tfrac{1}{2}\varepsilon_{yy}\,\phi_y^2, \tag{3}$$

where ϕ is the scalar potential, $\phi_y = \partial\phi/\partial y$ and ε_{yy} is the dielectric constant along the cell normal. The energy density of interaction between spontaneous polarization and the electric field field is given by

$$f_{\text{p}} = -(\mathbf{P}_1 + \mathbf{P}_2)\cdot\mathbf{E}. \tag{4}$$

The bulk free energy density is given by

$$f_{\text{B}} = f_{\text{elas}} + f_{\text{c}} + f_{\text{d}} + f_{\text{p}}. \tag{5}$$

We assume that the layer structure is bookshelf and take the z axis along the layer normal and the y axis along the cell normal. Then,

$$\mathbf{k} = (0, 0, 1),\ \mathbf{c}_i = (\cos\Phi_i, \sin\Phi_i, 0),\ \mathbf{p}_i = (-\sin\Phi_i, \cos\Phi_i, 0), \tag{6}$$

where $\mathbf{p}_i$ is the unit vector along P_i and Φ_i is the angle between the x axis and $\mathbf{c}_i (i = 1, 2)$. We consider the one dimensional problem, i.e. we assume that ϕ and Φ_i depend only on y. Then, in this geometry,

$$f_{\text{elas}} = \sum_{i=1}^{2} (\tfrac{1}{4}(B_1\sin^2\Phi_i + B_2\cos^2\Phi_i)\Phi_{iy}^2 + \tfrac{1}{2}D_1\Phi_{iy}\sin\phi_i), \tag{7}$$

$$f_{\text{c}} = \tfrac{1}{4}\alpha P_{\text{s}}^2\cos(\Phi_1 - \Phi_2), \tag{8}$$

$$\varepsilon_{yy} = \frac{\varepsilon_2}{2}\sum_{i=1}^{2}(1 + e\sin^2\Phi_i),\ e = \frac{(\varepsilon_1\cos^2\theta + \varepsilon_3\sin^2\theta - \varepsilon_2)}{\varepsilon_2}, \tag{9}$$

$$f_{\text{p}} = \sum_{i=1}^{2}\left(-\frac{P_{\text{s}}}{2}\mathbf{p}_i\cdot\mathbf{E}\right) = \sum_{i=1}^{2}\frac{P_{\text{s}}}{2}\cos\Phi_i\ \phi_y. \tag{10}$$

In equation (7), $\Phi_{iy} = \partial\Phi_i/\partial y$. In equation (9), ε_3, ε_2 and ε_1 are the principal values of the dielectric tensor along the **n** director, the polarization vector and the direction perpendicular to them, respectively, and θ is the tilt angle of the **n** director with respect to the layer normal.

As the surface anchoring energy, we take the following functions;

$$\left.\begin{aligned} f_s^0 &= \gamma_0^1(\sin\xi^0 - \sin\beta^0)^2 - \gamma_2^0(p^0\cdot s^0), \\ f_s^d &= \gamma_1^d(\sin\xi^d - \sin\beta^d)^2 - \gamma_2^d(p^d\cdot s^d), \end{aligned}\right\} \tag{11}$$

where superscripts 0 and d denote the lower and upper surfaces, respectively, and **s** denotes the outward normal of the surface. In equation (11), the first and the second terms are the non-polar and the polar anchoring energies. $\xi^{0,d}$ is the angle between the **n** director at the surface and the surface plane (the xz plane), and $\beta^{0,d}$ is the surface pretilt angle of the **n** director. In the present case, $\sin\xi^{0,d} = \sin\theta\sin\Phi_i^{0,d}$, $p^0\cdot s^0 = \cos\Phi_i^0$ and $p^d\cdot s^d = -\cos\Phi_i^d$.

Using equations (7), (8), (9), (10) and (11) and the torque balance equation, dynamic equations with respect to $\Phi_i(y,t)$ are obtained.

$$\lambda\frac{\partial\Phi_i}{\partial t} = -\frac{\partial f_B}{\partial\Phi_i} + \frac{\partial}{\partial y}\frac{f_B}{\partial\Phi_{iy}} \quad \text{(in the bulk)}, \tag{12}$$

$$\frac{\partial f_B}{\partial\Phi_{iy}} = \frac{\partial f_s^0}{\partial\Phi_i} \quad \text{(at the lower surface)}, \tag{13}$$

$$\frac{\partial f_B}{\partial\Phi_{iy}} = -\frac{\partial f_s^d}{\partial\Phi_i} \quad \text{(at the upper surface)}. \tag{14}$$

In equation (12), λ is the rotational viscosity coefficient when the **n** director moves over the cone of cone angle 2θ. In equations (13) and (14), we assume a static torque balance at the surfaces. Applying the Euler–Lagrange equation with respect to scalar potential ϕ, we obtain the Poisson equation as

$$\frac{\partial}{\partial y}\left(\frac{\varepsilon_2}{2}\{2+e(\sin^2\Phi_1+\sin^2\Phi_2)\}\phi_y\right) = -\frac{P_s}{2}(\Phi_{1y}\sin\Phi_1 + \Phi_{2y}\sin\Phi_2). \tag{15}$$

The right hand side of equation (15) contributes to the polarization electric field [7, 8]. If we neglect this term and the dielectric anisotropy ($e=0$), ϕ is a linear function of y and the electric field is constant throughout the sample.

3. Results and discussion

To solve the set of equations (12)–(15), we resort to the conventional difference method for the space (y) and time (t) derivatives. The number of divisions along the y axis is 20. Once $\Phi_1(y,t)$ and $\phi_2(y,t)$ are obtained, we can calculate the relevant quantities such as the polarization reversal current, optical transmission, etc.

In the following calculations, we neglect the effect of polarization electric field, anisotropy of the dielectric constants and anisotropy of the elastic constants. We also neglect the polar anchoring strength. Values of parameters used in these calculations are as follows: tilt angle $\theta = 20°$, spontaneous polarization $P_s = 50\,\text{nC cm}^{-2}$, dielectric constants $\varepsilon_1 = \varepsilon_2 = \varepsilon_3 = 5{\cdot}0\varepsilon_0$ where ε_0 is the dielectric constant of a vacuum, elastic constants $B_1 = B_2 = 1{\cdot}66\times10^{-9}$ N, $D_1 = 0$, rotational viscosity $\lambda = 2{\cdot}6$ N.s m^{-1}, and pretilt angle of the **n** director at the surface $\beta_0 = 3{\cdot}62°$.

First, we calculate the apparent optical tilt angle θ_{app} as a function of applied DC voltage. This can be evaluated by calculating the optical transmission, with rotation of the cell between crossed polarizers, by means of the 4×4 matrix method [9]. The

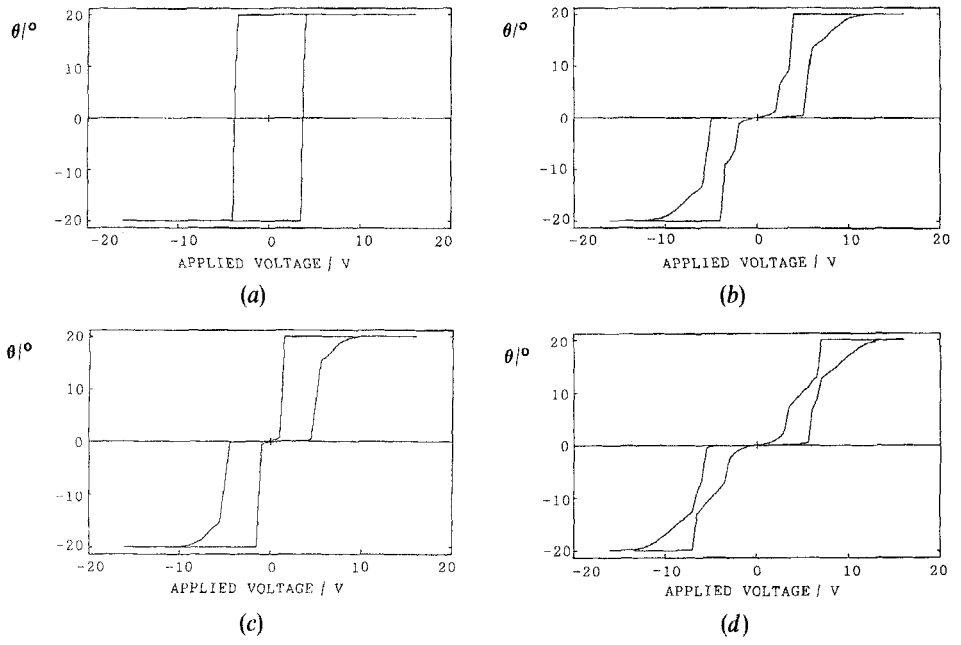

Figure 1. Apparent tilt angle versus applied DC voltage when the antiferroelectric coupling parameter is: (*a*) $\alpha' = 0$, (*b*) $\alpha' = 4$, (*c*) $\alpha' = 5$ and (*d*) $\alpha' = 6$.

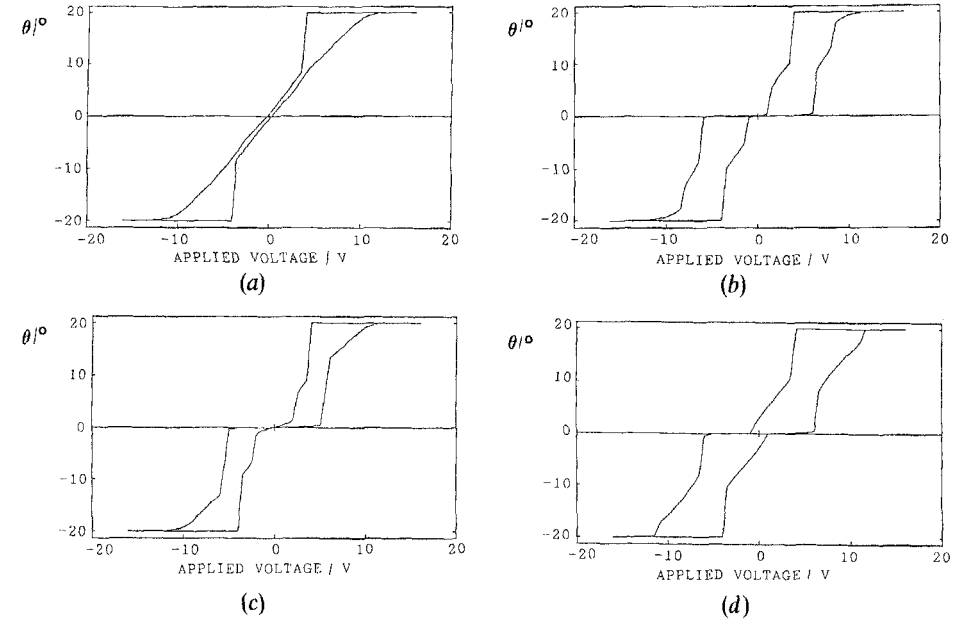

Figure 2. Apparent tilt angle versus applied DC voltage for different values of the non-polar surface anchoring strength. (*a*) $\gamma_1 = 0{\cdot}32 \times 10^{-3}\,\mathrm{N\,m^{-1}}$, (*b*) $\gamma_1 = 0{\cdot}96 \times 10^{-3}\,\mathrm{N\,m^{-1}}$, (*c*) $\gamma_1 = 1{\cdot}60 \times 10^{-3}\,\mathrm{N\,m^{-1}}$, (*d*) $\gamma_1 = 2{\cdot}24 \times 10^{-3}\,\mathrm{N\,m^{-1}}$.

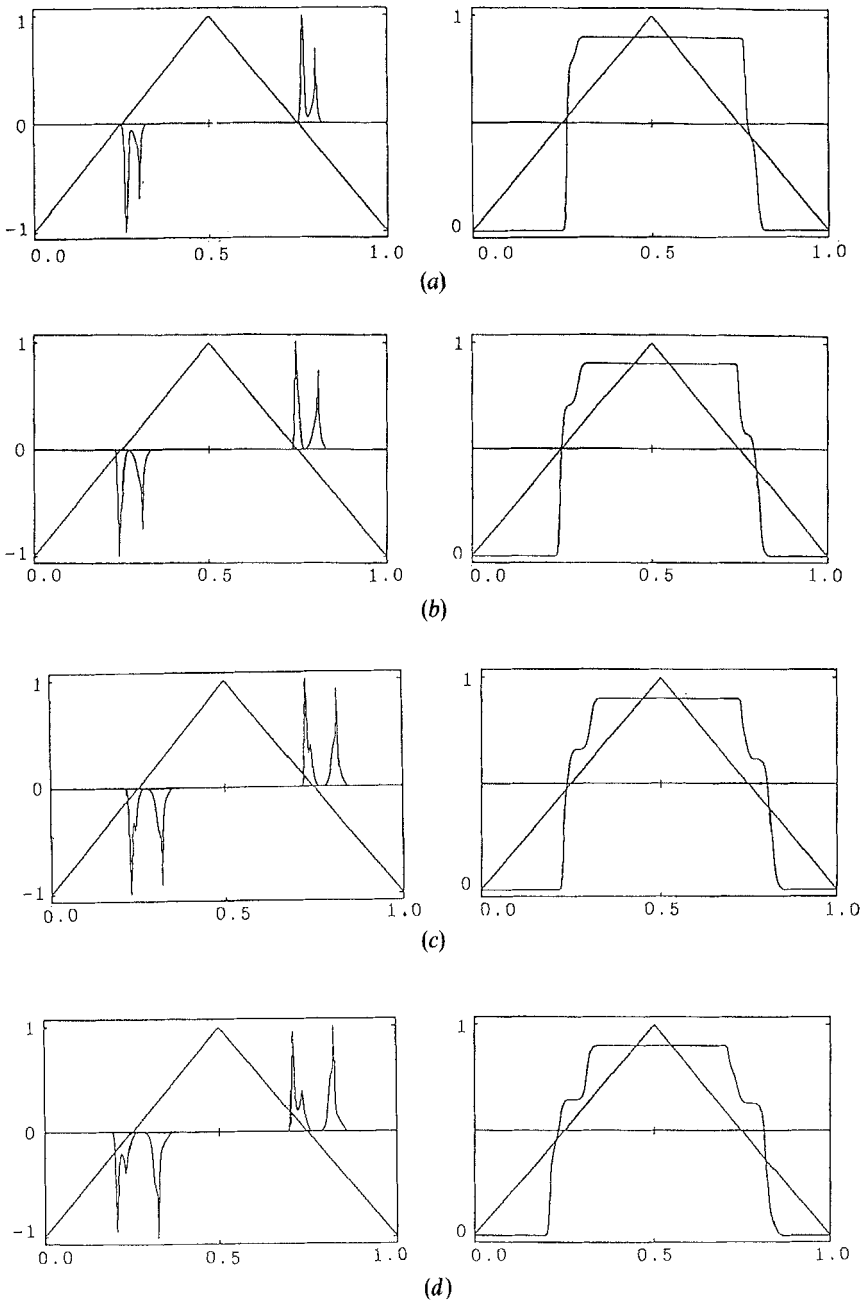

Figure 3. Polarization reversal current (left column) and optical transmission (right column) between crossed polarizers for different values of the antiferroelectric coupling parameter when triangular wave voltages are applied. (*a*) $\alpha' = 3$, (*b*) $\alpha' = 4$, (*c*) $\alpha' = 5$, (*d*) $\alpha' = 6$.

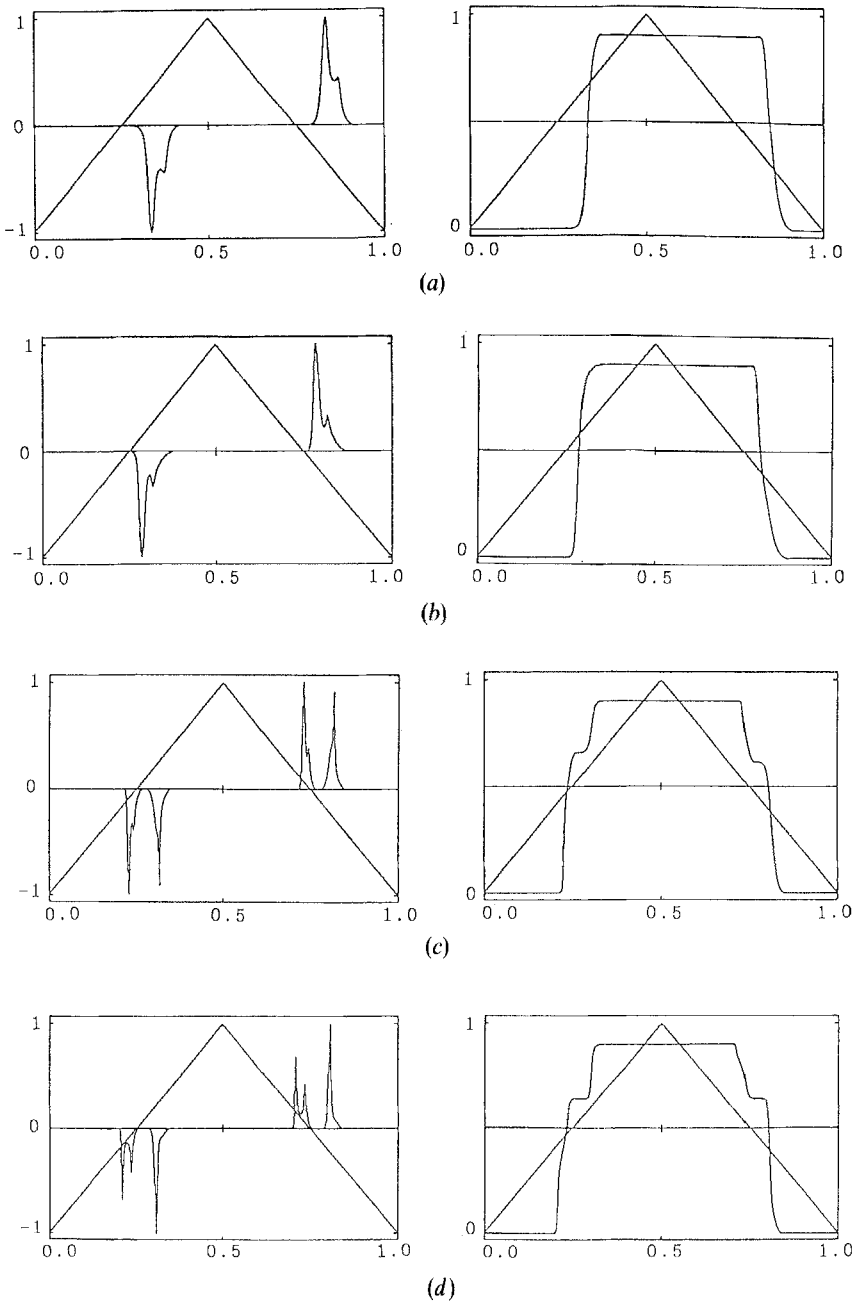

Figure 4. Polarization reversal current (left column) and optical transmission (right column) between crossed polarizers for different values of the frequency when triangular wave voltages are applied. (*a*) $f=160$ Hz, (*b*) $f=80$ Hz, (*c*) $f=20$ Hz, (*d*) $f=10$ Hz.

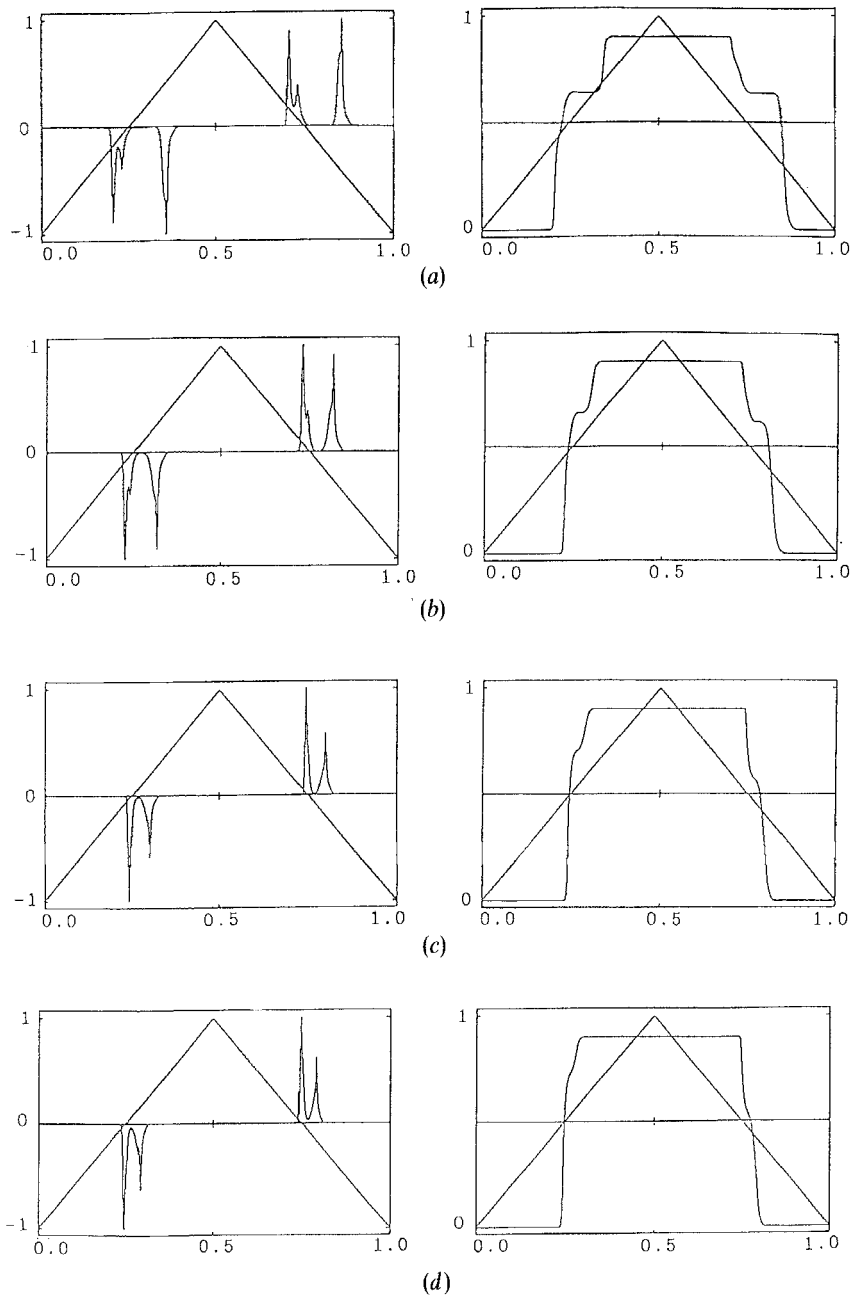

Figure 5. Polarization reversal current (left column) and optical transmission (right column) between crossed polarizers for different values of the amplitude of the voltage when triangular wave voltages are applied. (*a*) $V=20$ V, (*b*) $V=30$ V, (*c*) $V=40$ V, (*d*) $V=50$ V.

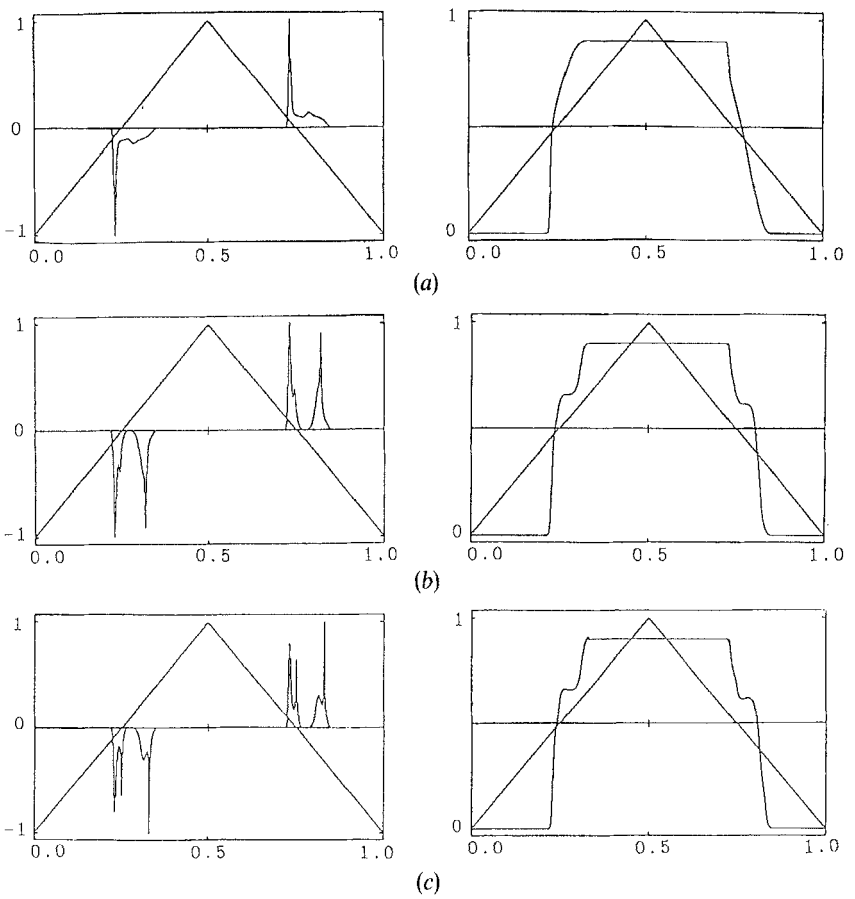

Figure 6. Polarization reversal current (left column) and optical transmission (right column) between crossed polarizers for different values of the non-polar surface anchoring strength when triangular wave voltages are applied. (*a*) $\gamma_1 = 0{\cdot}32 \times 10^{-3}\,\mathrm{N\,m^{-1}}$, (*b*) $\gamma_1 = 0{\cdot}96 \times 10^{-3}\,\mathrm{N\,m^{-1}}$, (*c*) $\gamma_1 = 1{\cdot}60 \times 10^{-3}\,\mathrm{N\,m^{-1}}$.

results are shown in figures 1 and 2. Figure 1 shows the effects of the antiferroelectric coupling parameter $\alpha' = \alpha\varepsilon_2$ when the non-polar surface anchoring strength is fixed to the value $\gamma_1 = 0{\cdot}96 \times 10^{-3}\,\mathrm{N\,m^{-1}}$. When $\alpha' = 0$, the ferroelectric phase is stabilized and the θ_{app} versus V curve exhibits the single hysteresis (figure 1 (*a*)) characteristic of ferroelectric liquid crystal phases. When $\alpha' > 0$, a double hysteresis is observed. The threshold voltage of the electric field induced transition from an antiferroelectric phase to one of the uniform ferroelectric states becomes higher, as α' becomes larger. α' is considered to become larger as the temperature is lowered. Therefore, this tendency agrees with the experimental results for TFMHPOBC [3]. Figure 2 shows the effects of non-polar surface anchoring strength, when α' is fixed to $\alpha' = 5$. When γ_1 is small see figure 2 (*a*)), the threshold for the electric field induced transition from an antiferroelectric phase to one of the uniform ferroelectric states disappears. The hysteresis loop becomes wider as γ_1 becomes larger.

The polarization reversal current is calculated by

$$I_p = \frac{\partial}{\partial t}\left\{\frac{P_s}{2}\left(\langle\cos\Phi_1\rangle + \langle\cos\Phi_2\rangle\right)\right\}, \tag{16}$$

where $\langle \cos \Phi_i \rangle$ is given by

$$\langle \cos \Phi_i \rangle = \frac{1}{d} \int_0^d \cos \Phi_i \, dy .$$

The dynamic response of the optical transmission using crossed polarizers is calculated by means of the 4 × 4 matrix method. These results are shown for one period of applied triangular wave voltages in figures 3–6. In these figures the left hand columns show the polarization reversal currents in arbitrary units. Those in the right hand columns show the optical transmissions when the crossed polarizers are set so that one of the uniform ferroelectric states is in an extinct state. In general, the polarization reversal current exhibits double peaks, corresponding to the relaxation from one of the uniform ferroelectric states to the antiferroelectric state, and the electric field induced transition from the antiferroelectric state to the other uniform ferroelectric state. The optical transmission also exhibits this tristable switching. Figure 3 shows the effect of α' when $\gamma_1 = 0{\cdot}96 \times 10^{-3}\,\mathrm{N\,m^{-1}}$, $V = 30\,\mathrm{V}$ and the frequency $f = 20\,\mathrm{Hz}$. When α' becomes larger, the spacing between the double peaks becomes wider as is expected. The effects of the frequency of the applied voltages are shown in figure 4, when $\alpha' = 5$, $\gamma_1 = 0{\cdot}96 \times 10^{-3}\,\mathrm{N\,m^{-1}}$ and $V = 30\,\mathrm{V}$. As the frequency becomes higher, the spacing between the double peaks becomes smaller and finally only a single peak appears in the polarization reversal current (see figures 4 (*a*) and (*b*)). This means that bistable switching occurs between uniform ferroelectric states without passing through the antiferroelectric state. This phenomenon corresponds to the single hysteresis loop in *D*–*E* curves at high frequencies which is experimentally observed [2]. The effects of the amplitude of the applied voltages are shown in figure 5, when $\alpha' = 5$, $\gamma_1 = 0{\cdot}96 \times 10^{-3}\,\mathrm{N\,m^{-1}}$ and $f = 20\,\mathrm{Hz}$. As the voltage becomes higher, the spacing between the double peaks becomes smaller as was the case for the frequency dependence. Finally, figure 6 shows the effect of the non-polar surface anchoring strength when $\alpha' = 5$, $V = 30\,\mathrm{V}$ and $f = 20\,\mathrm{Hz}$. When γ_1 is small, the second peak in the polarization reversal current is merged with the first peak (see figure 6 (*a*)). When γ_1 is large, both the first and the second peaks split into two peaks (see figure 6 (*c*)). This is due to the delay of the polarization reversal near the surfaces with respect to that in the bulk.

4. Conclusions

Responses of surface stabilized antiferroelectric liquid crystals (SSAFLCs) to an electric field were simulated based on a model of the AFLC phase in which its structure was assumed to consist of two ferroelectric S_C^* sublattices paired by antiferroelectric coupling. The apparent tilt angle, the polarization reversal current and the optical transmission under applied triangular wave voltages were calculated. The results obtained explain the experimental observations fairly well. As the antiferroelectric coupling parameter becomes larger (this corresponds to lower temperatures), the threshold DC voltage of the electric field induced transition from the antiferroelectric state to one of the uniform ferroelectric states becomes higher and the spacing between the double peaks in the polarization reversal current becomes wider. These are natural results, because the antiferroelectric phase is more stable when the antiferroelectric coupling parameter is larger. When the amplitude and frequency of the applied triangular wave voltages become higher, the spacing between the double peaks in the polarization reversal current becomes smaller. Especially, when the frequency is high, only a single peak appears due to the direct transition from one of the uniform

ferroelectric states to the other. It was also shown that the surface anchoring strength has crucial effects on switching characteristics.

References

[1] CHANDANI, A. D. L., OUCHI, Y., TAKEZOE, H., FUKUDA, A., TERASHIMA, K., FURUKAWA, K., and KISHI, A., 1989, *Jap. J. appl. Phys.*, **28,** L1261.
[2] ORIHARA, H., FUJIKAWA, T., ISHIBASHI, Y., YAMADA, Y., YAMAMOTO, N., MORI, K., NAKAMURA, K., SUZUKI, Y., HAGIWARA, T., and KAWAMURA, I., 1990, *Jap. J. appl. Phys.*, **29,** L333.
[3] INUI, S., KAWANO, S., SAITO, M., IWANE, H., TAKANISHI, Y., HIRAOKA, K., OUCHI, Y., TAKEZOE, H., and FUKUDA, A., 1990, *Jap. J. appl. Phys.*, **29,** L987.
[4] CHANDNI, A. D. L., HAGIWARA, T., SUZUKI, Y., OUCHI, Y., TAKWZOE, H., and FUKUDA, A., 1988, *Jap. J. appl. Phys.*, **27,** L729.
[5] NAKAGAWA, M., 1988, *Jap. J. appl. Phys.*, **30,** 1759.
[6] DAHL, I., and LAGERWALL, S. T., 1984, *Ferroelectrics*, **58,** 215.
[7] NAKAGAWA, M., and AKAHANE, T., 1986, *J. phys. Soc. Japan*, **55,** 1516.
[8] NAKAGAWA, M., and AKAHANE, T., 1986, *J. phys. Soc. Japan*, **55,** 4429.
[9] BERREMAN, D. W., 1992, *J. opt. Soc. Am.*, **62,** 502.